PCCP

PAPER

View Article Online
View Journal | View Issue

Cite this: *Phys. Chem. Chem. Phys.*, 2020, **22**, 11490

Reactivity and rotational spectra: the old concept of substitution effects†

Sven Herbers, *[a] Philipp Buschmann, [a] Juan Wang,[ab] Kevin Gregor Lengsfeld,[a] K. P. Rajappan Nair[ac] and Jens-Uwe Grabow [a]

Received 28th February 2020,
Accepted 25th April 2020

DOI: 10.1039/d0cp01145b

rsc.li/pccp

The internal rotation of methyl groups and nuclear quadrupole moments of the halogens Cl, Br, I in *o*-halotoluenes cause complex spectral fine and hyperfine structures in rotational spectra arising from angular momentum coupling. Building on the existing data regarding *o*-fluorotoluene and *o*-chlorotoluene, the investigations of *o*-bromotoluene and *o*-iodotoluene allow for a complete analysis of the homologous series of *o*-halogenated toluenes. The trend in the methyl barriers to internal rotation rising with the size of the halogen can be rationalised by repulsion effects as predicted by MP2 calculations. Furthermore, the analysis of the observed quadrupole coupling serves as a quantitative intra-molecular probe, *e.g.* for the explanation of the relative reaction yields in the nitration of halotoluenes, related to the different π-bond character of the C–X bond depending on the position of substitution.

1 Introduction

Even in the rising era of computational chemistry, the intuitive understanding of product formation in organic reactions, including the classic concept of substitution effects, is of considerable importance. In the field of synthesising highly functionalised aromatic systems, that are of pharmaceutical importance, a precise idea about the electronic influences of the substituents already introduced into the molecule guides the selection of a suitable synthesis route. For these systems, rules were empirically established from analysing yields of various electrophilic substitutions of substituted benzenes. These concepts were mainly introduced by Robinson and Ingold and applied in countless publications and are still part of the basic course in organic chemistry for undergraduate students.[1] One common example is the nitration of aromatic molecules like toluene, where the formation of *o*- an *p*-nitrotoluene is preferred over *m*-nitrotoluene caused by the directing inductive influence of the methyl group. The preferred products are usually explained with the possible resonance structures of the intermediate cation formed after the electrophilic attack. Only for *o*- and *p*-attack a cation with the positive charge next to the electron donating methyl group can be formed as illustrated in Fig. 1(a). The electron pulling or electron pushing effect of substituents through the σ bond system is commonly referred to as inductive (−/+I) effect. For halogenated benzenes it might be expected that electrophilic substitution is preferred

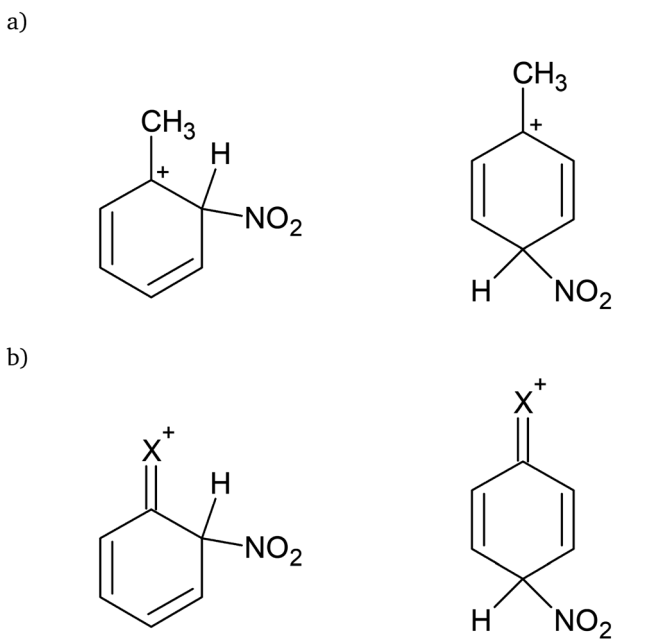

Fig. 1 Stabilised intermediate cations after electrophilic attack of NO_2^+ on *o*- and *p*-position for (a) toluene (b) halobenzene.

[a] *Institut für Physikalische Chemie und Elektrochemie, Leibniz Universität Hannover, 30167 Hannover, Germany. E-mail: sven.herbers@pci.uni-hannover.de*
[b] *Department of Chemistry, Chongqing University, 401331 Chongqing, China*
[c] *Department of Atomic and Molecular Physics, Manipal Academy of Higher Education, 576104 Manipal, India*

† Electronic supplementary information (ESI) available: All SPFIT and XIAM fit output files and all quantum chemical frequency calculation outputs that are referred to in the article, as well as a detailed discussion of product yields. See DOI: 10.1039/d0cp01145b

on *meta*-positions over *ortho*- and *para*-positions, since the halogen is pulling electrons out of the ring (−I), and a positive charge next to the halogen would not be preferred. However, the halogen substituents are *ortho*- and *para*-position directing, whereby their −I effect simultaneously reduces the reaction rate. This, in the Lewis structure model, is explained by the lone pairs of the halogen, that can form a double bond to the ring carbon atom corresponding to a resonance structure, which leaves a positive charge at the halogen, illustrated in Fig. 1(b). This is commonly referred to as mesomeric effect (−/+M).[1,2]

To study the influence of inductive and mesomeric effects in the absence of any electrophile experimentally, supersonically cooled jet-expansion techniques combined with high-resolution microwave spectroscopy are excellently suited to test and quantify these concepts: for the halogens chlorine, bromine and iodine, the ranking in −I as well as +M effects is Cl > Br > I. This is rationalised by the decreasing electronegativity as well as orbital overlap regarding the carbon they bind to. Since these nuclei do have an electric quadrupole moment, information on the electronic environment, *i.e.* their bonding situation, can be obtained from their quadrupole coupling tensor, derived from the hyperfine structure in rotational spectra. From the symmetry of the quadrupole coupling tensor as well as the magnitude of its elements, the population of the valence p-orbitals can be derived and deviations directly reflect the strength of a possible +M and −I effect. In previous investigations of halobenzenes[3] and the homologues of the *p*-halotoluenes[4] the trend Cl > Br > I for both, +M and −I effects was verified. This study extends and completes the series of *o*-halotoluenes by measurements on *o*-bromotoluene and *o*-iodotoluene. In addition, the rather large barrier to internal rotation of the methyl group in *o*-halotoluenes will be discussed in this study.

2 Model Hamiltonian

To derive precise molecular parameters from spectra, an effective model Hamiltonian has to be employed. In many cases a satisfying description of the rotational motion of a molecule can be achieved by using a semi rigid model (Watson's *S* reduction in I^r representation[5]):

$$H_{sr} = H_{rr} + H_{cd} \quad (1)$$

$$H_{rr} = A_0 P_a^2 + B_0 P_b^2 + C_0 P_c^2 \quad (2)$$

$$H_{cd} = -D_J P^4 - D_{JK} P^2 P_a^2 - D_K P_a^4 + d_1 P^2 (P_+^2 + P_-^2) + d_2 (P_+^4 + P_-^4) \quad (3)$$

In this semi rigid model (sr), the rotation is treated separately from vibrational motions as a rigid rotor (rr), corrected for centrifugal distortion (cd). A_0, B_0, C_0 are the ground vibrational state rotational constant, P_a, P_b, P_c the components of the angular momentum operator. D_J, D_{JK}, D_K, d_1, and d_2 are the quartic centrifugal distortion coefficients, $P_\pm = P_b \pm iP_c$ are commonly known as ladder or step operators. However, in the presence of methyl groups the coupling between the internal rotation along a threefold potential energy path and the overall rotation of the molecule often becomes significant. The semi rigid model is then expanded by an internal rotation H_i term, which includes the coupling:

$$H = H_{sr} + H_i \quad (4)$$

$$H_i = F(p_\alpha - \boldsymbol{\rho}\mathbf{P})^2 + \frac{V_3}{2}(1 - \cos(3\alpha)) \quad (5)$$

Here, the constant

$$F = \frac{F_0}{r} = \frac{\hbar^2}{2rI_\alpha} \quad (6)$$

is the reduced constant of internal rotation. V_3 is the barrier for the threefold internal rotation and α is the torsional angle. In the limiting case of vanishing coupling F can be derived from the structural moment of inertia of the methyl top I_α but in general the effect of coupling is taken into account by the reducing factor $r = 1 - \sum_i \frac{\lambda_i^2 I_\alpha}{I_i}$ with λ_i being the direction cosines for the internal rotation axis with respect to the principal axes i. F_0, which is the structural constant to internal rotation directly derived from I_α, can easily be estimated from quantum chemically optimised molecular geometries to be about 161.6 GHz for all *o*-halogenated toluenes. The vector $\boldsymbol{\rho}$ with $\rho_i = \lambda_i \frac{I_\alpha}{I_i}$ in eqn (5) gives rise to cross-terms originating from the coupling between internal and overall rotation. Its absolute value ranges between zero and one. The zero-value of $|\boldsymbol{\rho}| = 0$ marks the limiting case of vanished coupling. For $|\boldsymbol{\rho}| = 0$ the internal rotation part would simply lead to a set of energy levels on the potential energy curve along the torsional degree of freedom. These can be labelled either by $\pm m$ quantum numbers, commonly used for small barriers to internal rotation, where the eigenstates are close to free rotor states, or at larger barriers by their torsional vibration v quantum numbers. In this article we will follow the latter labelling scheme. With a finite barrier that allows for tunnelling, the v levels will be split into two symmetry species, labelled with their symmetry quantum number $\sigma = 0, \pm 1$. Levels with $\sigma = 0$ are referred to as A species and levels with $\sigma = \pm 1$ are referred to as E species. Transitions from A to E species are forbidden, so that for $|\boldsymbol{\rho}| = 0$ no splittings would arise in the rotational spectrum, since there is no coupling between rotation and internal rotation. For non vanishing $|\boldsymbol{\rho}|$ values the spectrum will be split and each transition can be assigned to a symmetry species.

Treatment of the internal rotation part of the Hamiltonian is usually carried out using one of three methods: principal axis method PAM, ρ-axis method RAM, or the combined axis method CAM, which combines PAM and RAM. A more thorough description of PAM and RAM can be found in ref. 6 and 7. Detailed information on state of the art programs to treat internal rotation problems is given in the review written by Kleiner.[8]

Further complications arise if the molecule contains a nucleus with electric quadrupole moment. A non-zero electric field gradient at the nucleus together with a significant nuclear quadrupole moment causes strong coupling between nuclear

spin and overall rotation of the molecule. The Hamiltonian is then expanded by another term (q):

$$H = H_{sr} + H_i + H_q \quad (7)$$

Matrix elements of H_q are provided in ref. 9. The elements of H_q are parametrised by the matrix elements of the quadrupole coupling tensor χ, which can be derived from the hyperfine structure of a rotational spectrum. In its diagonalised form, the tensor elements are proportional to the quadrupole moment Q of the nucleus:

$$\chi_{ii} = eq_{ii}Q \quad (8)$$

Here e is the proton charge and q_{ii} is the electric field gradient at the nucleus. Although exact treatment is possible, elements off-diagonal in J are often omitted for simplicity. Omitting the off-diagonal elements does cause errors, that, in the case of rather small quadrupole moments (like nitrogen or deuterium nuclei) in absence of near-degeneracies, are usually small compared to experimental accuracy. However, chlorine, bromine, and iodine containing compounds can not be treated properly by this approach and are strongly affected by coupling of quadrupolar nuclei. The popular program XIAM,[10–13] which uses the CAM method, does not include elements off-diagonal in J. Consequently, quadrupolar coupling can not be treated with experimental accuracy in XIAM for the case of the *o*-halotoluenes investigated in this study. Instead we will utilise a two step procedure as proposed in the study of $(CH_3)SiI$.[14] In a first step the internal rotation symmetry species A and E are treated separately in terms of the PAM utilizing the program SPFIT, which treats quadrupolar coupling exactly. In the high barrier regime, this yields fits with experimental accuracy. In a second step the effects of quadrupolar coupling are removed and the hyperfine structure free line list of hypothetically unsplit centre frequencies is used in a fit with XIAM to derive the internal rotation parameters and structural rotational constants. While experimental accuracy fits were possible with SPFIT using effective parameters, these lack easy interpretation. Therefore, XIAM was preferred and used for the derivation of internal rotation parameters.

3 Computational

All calculations were carried out with Gaussian16 (Revision A.03).[15] All *o*-halotoluenes optimisations with subsequent frequency calculations were performed using the B3LYP[16–19] and the MP2[20] method with a 6-311++G(2d,2p) basis set as implemented in Gaussian. For iodine a 6-311G** basis set[21] taken from the EMSL basis set exchange library[22] (https://bse.pnl.gov/bse/) was used. In addition MP2 relaxed potential energy surface scans were performed to predict the internal rotation barrier. Additionally, MP2 calculations on halobenzenes and *p*-halotoluenes were carried out to consistently predict the π-bond character of the halogen–carbon bonds and compare the results with those obtained for the *o*-halotoluenes. For *o*-iodotoluene the influence of relativistic effects on the C–I bond length was estimated by comparing an MP2(full) optimisation with an MP2(full) optimisation using the Douglas–Kroll–Hess second-order scalar relativistic (dkh) Hamiltonian.[23–26]

4 Experimental

A commercial sample of *o*-bromotoluene (Aldrich, 99%) was used without further purification. Gas mixtures of $\approx$5 mbar in 4 bar of helium were prepared and measurements were carried out with the coaxially oriented beam resonator arrangement Fourier transform microwave (COBRA-FTMW) spectrometer in Hannover.[27] Segments of the spectrum were recorded between 5 and 21 GHz. From the recorded signals, 190 were identified to belong to the ^{79}Br isotopologue and 240 belong to the ^{81}Br isotopologue. For the investigations of *o*-iodotoluene, a commercial sample (Alfa Aesar, 98%) was placed into a custom made reservoir nozzle on the broad band inphase/quadrature-phase modulation passage-acquired-coherence technique (IMPACT-FTMW) spectrometer.[28] The spectrum from 8.5–18.5 GHz was recorded with neon as carrier gas. The sample was heated up to 70 °C by a resistive coil, wrapped around the nozzle head. 1093 signals were identified from the spectrum and assigned to *o*-iodotoluene. In both experiments the backing pressure was 1 bar. Fits of molecular parameters to experimental frequencies were carried out using SPFIT[29] and XIAM.[10–13] In the XIAM fits the values of F_0 were fixed on values of the B3LYP optimised equilibrium geometries. An example for a well resolved quadrupole and internal rotation split transition is given in Fig. 2 for *o*-bromotoluene. All transitions are Doppler-split since the coherently rotating ensemble of molecules emits parallel and anti-parallel to the propagation direction of the molecular jet with both components detected.

5 Results and discussion

5.1 *o*-Fluorotoluene

o-Fluorotoluene was already investigated in ref. 30, but the presented fits are rather problematic. Instead of fitting A and E species with the same weight, primarily the deviation of the A species was minimised, which is reflected in the rather high deviations for E species lines up to 545 kHz. Also F_0 was fixed to a value, which is inconsistent with our values derived from B3LYP optimised geometries. Since V_3 and F_0 are strongly correlated, this would lead to barriers inconsistent with the barriers of the other *o*-halotoluenes investigated in this study. Therefore, we reanalysed the *o*-fluorotoluene measurements based on the line list presented in ref. 30. An overall standard deviation of σ = 3.0 kHz was achieved with a maximum deviation of 15 kHz and a barrier of 236.841(10) cm^{-1} was obtained.

5.2 *o*-Chlorotoluene

o-Chlorotoluene was subject of several spectroscopic investigations.[31–35] A reasonable barrier height based on microwave investigations with a COBRA-type spectrometer was determined in ref. 34 in terms of the principal axis method, providing a value of $V_{3,35Cl}$ = 466.44(43) cm^{-1} and $V_{3,37Cl}$ = 466.2(15) cm^{-1}.

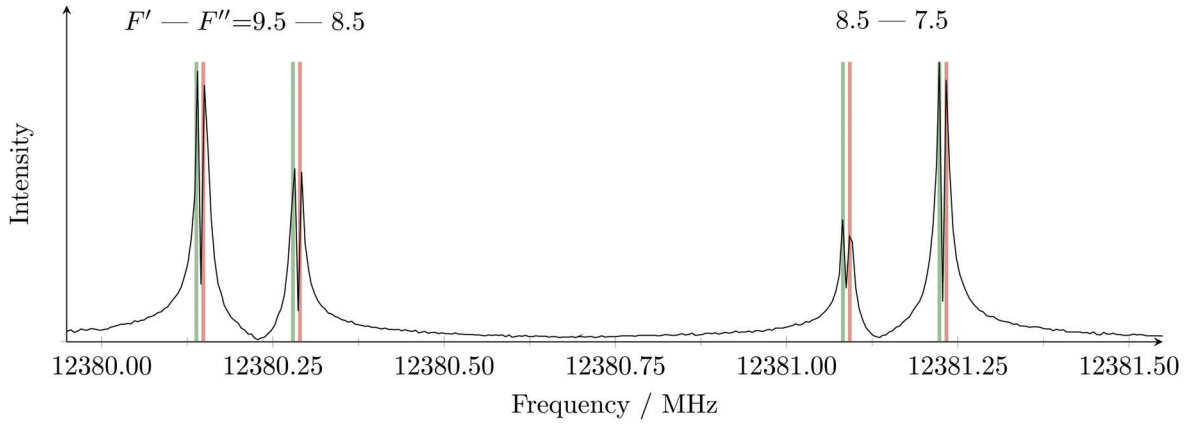

Fig. 2 Two of the hyperfine components of the $J'_{K'_aK'_c} - J''_{K''_aK''_c} = 8_{18} - 17_{17}$ transition of *o*-bromotoluene. Doppler pairs predicted from the parameters of the fit are coloured red for the *A* symmetry species and green for the *E* symmetry species. The separation between the two hyperfine components is 944 kHz, *A*/*E* splitting is 12 kHz while the Doppler splitting amounts to 141 kHz with helium as carrier gas.

The list of microwave transitions used in ref. 34 was expanded by millimetre wave transitions and a global fit was carried out yielding a barrier of about 513 cm^{-1}.[35] In this global fit the parameter F_0 was floated and took a value of 178.4 GHz for the ^{35}Cl isotopologue, corresponding to I_α = 2.833 amu Å^2, which is too small for a methyl group's moment of inertia. Taking the microwave data provided in ref. 34 we reanalysed the spectrum with the SPFIT+XIAM two step fitting procedure. In the XIAM fit we added the millimetre wave lines from ref. 35, for which no splitting due to quadrupole interaction was resolved. To facilitate the determination of accurate internal rotation barriers, only lines for which *A* as well as *E* species were provided are used. The fit shows excellent agreement between microwave ($\sigma_{mw,35Cl}$ = 1.3 kHz, $\sigma_{mw,37Cl}$ = 1.4 kHz) and millimetre wave ($\sigma_{mmw,35Cl}$ = 30.3 kHz, $\sigma_{mmw,37Cl}$ = 40.6 kHz) data. The deviations are consistent with the expected experimental accuracy of the microwave transitions of a few kHz and the millimetre wave transitions of about 100 kHz. The determined barriers $V_{3,35Cl}$ = 469.211(90) cm^{-1} and $V_{3,37Cl}$ = 469.863(204) cm^{-1} are in satisfactory agreement with each other. Besides the internal rotation, also the quadrupolar coupling can straightforwardly be analysed, since the $\chi_{yy} = \chi_{cc} = eq_{cc}Q$ component of the quadrupole coupling tensor will not change with rotation of the coordinate system around the *c*-axis due to the molecule's *a*,*b*-plane of symmetry. This invariance upon isotopic substitution allows a precise ratio determination of the quadrupole moments of both nuclei $\frac{Q_{35Cl}}{Q_{37Cl}} = \frac{\chi_{yy,35Cl}}{\chi_{yy,37Cl}} = 1.268745(66)$, without having to rely on the off-diagonal element of the tensor, which would otherwise be the largest source of uncertainty. This precise determination re-derived from the lines provided in ref. 34, which agrees with the recent values of Q_{35} = $-0.08165(80) \times 10^{-24}$ cm^2 and Q_{37} = $-0.06435(64) \times 10^{-24}$ cm^2 tabulated in ref. 36, resulting in a ratio of 1.2688(177).

5.3 *o*-Bromotoluene

o-Bromotoluene was not investigated by means of microwave spectroscopy before. However, internal rotation and bromine nuclear quadrupole coupling were dealt with in other molecules already, *e.g.* bromopropane[37] or, more closely related to this study, *p*-bromotoluene.[4] Since internal rotation splittings are small due to the high barrier in *o*-halotoluenes, the SPFIT-XIAM two step procedure achieves experimental accuracy. The barriers to internal rotation $V_{3,79Br}$ = 502.333(614) cm^{-1} and $V_{3,81Br}$ = 503.221(522) cm^{-1} are in good agreement. Again the ratio of the quadrupole moments $\frac{Q_{79Br}}{Q_{81Br}} = \frac{\chi_{yy,79Br}}{\chi_{yy,81Br}} = 1.19704(10)$ can be derived at high precision, and agrees with the ratio of the recommended quadrupole moments[36] of 1.1969(162).

5.4 *o*-Iodotoluene

Of the investigated halotoluenes, *o*-iodotoluene has the most pronounced quadrupole splitting. The barrier to internal rotation is $V_{3,I}$ = 530.004(136) cm^{-1}, which is in agreement with the trend to higher barriers with larger atom radii throughout the halogens. Since iodine has only one stable isotope, there is no ratio of quadrupole moments to be derived. Iodine has a very heavy nucleus, so that relativistic effects are expected to have a noticeable influence on the structure of the molecule. The relativistic effect on the C–I bond length was estimated using MP2(full)/6-311++G(2d,2p) calculations with and without DKH Hamiltonian. The inclusion of relativistic effects in the optimisation leads to a decrease in the C–I bond length of 6 mÅ.

5.5 Trend in the potential barrier

The trend in the potential barrier mainly reflects the exchange-repulsion of electrons between halogen and methyl rotor. The internal rotation parameters of all *o*-halotoluenes are summarised in Table 1. The barrier is monotonically increasing with the atomic number. The exchange-repulsion rising with the halogen's atomic size also affects the structure of the molecule in that the halogen enlarges its distance from the methyl rotor. This is best reflected in the angle φ between the two ring carbons and the halogen. In Fig. 3 the experimental results are plotted together with MP2 predictions, which reproduce the experimental values very well.

Table 1 Vibrational ground state structural rotational constants A_0, B_0, C_0 as well as barrier to internal rotation V_3 and angle δ between principal A axis and internal rotation axis α for all o-halotoluenes. The constant to internal rotation F_0 was fixed to values based on B3LYP equilibrium geometries, which is 161.6 GHz in all cases. Watson's S reduction in I^r representation was applied

	F	^{35}Cl	^{37}Cl	^{79}Br	^{81}Br	I
A_0/MHz	3243.09623(55)	2851.345869(119)	2842.55382(33)	2760.01069(162)	2758.95253(141)	2732.9609(24)
B_0/MHz	2180.49303(29)	1538.315441(41)	1500.290538(111)	989.236603(117)	978.929394(104)	738.409742(76)
C_0/MHz	1314.36349(14)	1005.370796(21)	987.925653(34)	731.461419(74)	725.736795(63)	583.394506(60)
F_0/GHz	161.6 (fixed)	161.6 (fixed)	161.6 (fixed)	161.6 (fixed)	161.6 (fixed)	161.6 (fixed)
δ/degree	29.307(14)	56.612(38)	57.159(80)	65.284(179)	65.146(152)	68.46(33)
V_3/cm^{-1}	236.841(10)	469.211(90)	469.86(21)	502.33(62)	503.22(53)	530.004(136)
N_{lines} [a]	86	524/430[c]	296/452[c]	190	240	1093
σ/kHz[b]	3.0	1.3/30.3[c]	1.4/40.6[c]	2.6	2.5	4.9

[a] Number of lines used in the fit. [b] Standard deviation of the fit. [c] cm wave and mm wave transitions, respectively.

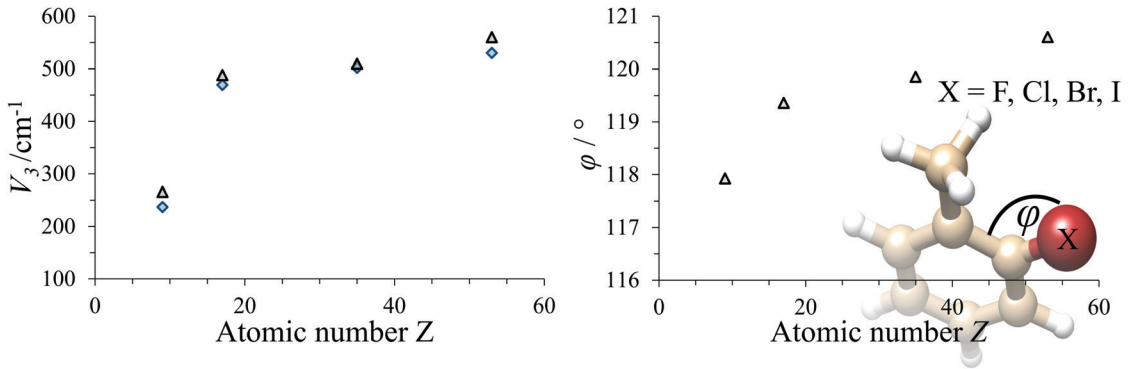

Fig. 3 Left: Dependence of V_3 on the atomic number Z of the halogen. Right: Dependence of the C–C–X angle φ on the atomic number of the halogen. Gray triangles: MP2 prediction, blue diamonds: experimental data.

5.6 Quadrupole coupling tensor – the character of the halogen bond

Townes and Dailey provided an intuitive and strikingly successful model to interpret the quadrupolar coupling tensor in terms of π-character (π_c) and ionic character (i_c) of chemical bonding.[38] For halogen substituents, that show approximately unaltered atomic p-orbitals, the relation

$$\begin{pmatrix} \chi_x & 0 & 0 \\ 0 & \chi_y & 0 \\ 0 & 0 & \chi_z \end{pmatrix} = n_x \begin{pmatrix} \chi_0 & 0 & 0 \\ 0 & -\frac{1}{2}\chi_0 & 0 \\ 0 & 0 & -\frac{1}{2}\chi_0 \end{pmatrix} + n_y \begin{pmatrix} -\frac{1}{2}\chi_0 & 0 & 0 \\ 0 & \chi_0 & 0 \\ 0 & 0 & -\frac{1}{2}\chi_0 \end{pmatrix} + n_z \begin{pmatrix} -\frac{1}{2}\chi_0 & 0 & 0 \\ 0 & -\frac{1}{2}\chi_0 & 0 \\ 0 & 0 & \chi_0 \end{pmatrix} \quad (9)$$

can be used to determine the populations n_g of the different p_g-orbitals with $g = x, y, z$.[39] The χ_g coefficients are elements of the diagonalised quadrupole coupling tensor and χ_0 is the quadrupole coupling constant due to a single valence p-electron, which can be found tabulated in ref. 6 (Table 14.2, for iodine see ref. 40). By convention, the z-axis points along the carbon–halogen σ-bond and we define, as being customary, the y-axis to be perpendicular to the ring plane. With the tensors being traceless only one additional assumption is necessary to solve eqn (9) for all n_g. Since any mesomeric effect caused by the halogen lone pairs will be reflected in a decrease of n_y, while n_x will remain rather unaffected, we assume its full occupation $n_x = 2.0$. The derived equations

$$n_y - n_x = \frac{2}{3}\left(\frac{\chi_z}{\chi_0}\right)\eta = \frac{2}{3}\left(\frac{\chi_x - \chi_y}{\chi_0}\right) \quad (10)$$

and

$$\frac{\chi_z}{\chi_0} + \frac{1}{2}(n_x + n_y) = n_z \quad (11)$$

are then used to determine n_y and n_z. $\eta = (\chi_x - \chi_y)/\chi_z$ is the asymmetry parameter for the quadrupole coupling tensor. The π-character is then simply the number of electrons removed from the p_y orbital

$$\pi_c = 4 - n_x - n_y \quad (12)$$

Table 2 C–X bond π-character π_c for selected holgenated aromatic molecules

X	*o*-X-Toluene	*m*-X-Toluene[42]	*p*-X-Toluene[4]	X-Benzene[3]
Cl	0.041_5	0.031	0.029	0.032
Br	0.040		0.023	0.025
I	0.039		0.017	0.019

and the ionic character is the excess of p-electrons

$$i_c = n_x + n_y + n_z - 5. \quad (13)$$

The ionic character can be related to the electronegativity x of the bonding atoms by the rough approximation[6,41]

$$i_c + \pi_c = i_\sigma = \frac{|x_X - x_{o\text{-Tol}}|}{2}, \quad (14)$$

for X = Cl, Br, I with respect to the group electro-negativity of the *o*-toluene fragment $x_{o\text{-Tol}}$. Here $i_\sigma = n_z - 1$ is the ionic character of the Sigma bond only. The results of the quadrupole coupling tensor analysis can thus be used to determine the group electro-negativity of the *o*-toluene fragment as presented in Table 4. In all cases π_c is rather small and about 4%. That π_c remains nearly constant under substitution is somewhat surprising, since for the halobenzenes as well as *p*-halotoluenes a decreasing trend with the size of the halogen is observed. The π_c values of the compounds are summarised in Table 2. The ionic character on the other hand changes from 30% for chlorine to 23% for bromine and 13% for iodine. This is similar to the trend in halobenzenes and *p*-halotoluenes which is reflected in constant values of group electronegativities for the aromatic ring fragments. A summary of the ionic character of different compounds and the derived fragment electronegativity is given in Table 3.

In the *o*-halotoluenes π_c increases with the introduction of the methyl group compared to the halobenzenes, while the *p*-halotoluenes show a decrease in π_c. While we can not give a simple explanation for this trend, MP2 calculations also predict a much higher π_c for *o*-halotoluenes. The MP2 predictions do not reproduce the constant behaviour within in *o*-halotoluenes, however, also in the bromine and iodine species of *p*-halotoluenes and halobenzenes π_c was underestimated compared to the chlorine values. If this systematic underestimation is taken into account the constant behaviour of the *o*-halotoluenes can be reproduced. The MP2 predictions of π_c are shown together with the experimental data in Fig. 4.

The trend in the ionic characters agrees with the tabulated electro-negativities[6] of 3.0 for chlorine, 2.8 for bromine and 2.55 for iodine, which were also used to derive the $x_{o\text{-Tol}}$ values of 2.32, 2.26 and 2.22. This slight variance of group electronegativities upon substitution was already observed in the case of halomethanes with values for chlorine, bromine and iodine containing species of 2.38, 2.30 and 2.29 for the methane

Table 3 C–X bond ionic character i_c and derived average electronegativity of the ring fragment $\bar{x}_{ring}$ for selected holgenated aromatic molecules

X	*o*-X-Toluene	*m*-X-Toluene[42]	*p*-X-Toluene[4]	X-Benzene[3]
Cl	0.30	0.30	0.31	0.30
Br	0.23		0.24	0.24
I	0.13		0.15	0.15
$\bar{x}_{ring}$	2.27	2.32[a]	2.27	2.27

[a] For chlorine substitution only. The value differs from the value of 2.39 presented in Table 5 of ref. 42, which we corrected for the π contribution to the ionic character.

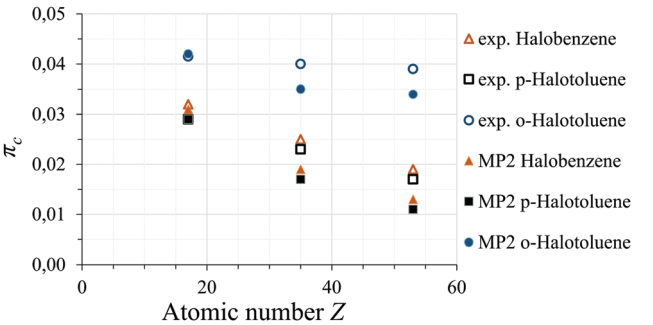

Fig. 4 π-Character π_c for halobenzenes (triangles), *p*-halotoluenes (squares), and *o*-halotoluenes (circles): MP2-predicted (filled shapes) and experimental (empty shapes) results.

Table 4 Quadrupole coupling tensor elements χ obtained from PAM fits using SPFIT. The symmetric quadrupole coupling tensor with corresponding elements χ_{aa}, χ_{bb}, χ_{cc}, and χ_{ab} was diagonalised to yield $\chi_{x,y,z}$. The angle θ between the two axis systems (between *a*- and *z*-axis) as well as orbital populations $n_{x,y,z}$, π-bond character π_c, ionic character i_c as well as the group electronegativity of the *o*-toluene fragment $x_{o\text{-Tol}}$ are derived from the tensor elements

	^{35}Cl	^{37}Cl	^{79}Br	^{81}Br	I
$\frac{3}{2}\chi_{aa}$/MHz	−101.9576(14)	−80.8330(14)	822.148(14)	686.869(11)	−2796.915(16)
$\frac{1}{4}(\chi_{bb} - \chi_{cc})$/MHz	1.21326(43)	1.03494(46)	−11.4749(67)	−9.5947(62)	33.4838(71)
χ_{ab}/MHz	14.98(28)	10.20(29)	12.33(49)	7.41(14)	−27.259(26)
χ_z/MHz	−70.079	−55.125	548.279	457.990	−1864.869
χ_x/MHz	38.520	30.251	−297.179	−248.223	999.532
χ_y/MHz	31.559	24.874	−251.100	−209.767	865.337
n_z	1.340	1.342	1.268	1.268	1.167
n_x	2.000	2.000	2.000	2.000	2.000
n_y	1.958	1.959	1.960	1.960	1.961
π_c	0.042	0.041	0.040	0.040	0.039
i_c	0.298	0.301	0.228	0.228	0.128
$x_{o\text{-Tol}}$	2.320	2.316	2.264	2.264	2.216
θ/degree	8.007	6.912	0.836	0.601	0.545

Table 5 Ratios of chlorine and bromine quadrupole moments derived in different studies

	o-X-Tol.	*m*-X-Tol.[42]	*p*-X-Tol.[4]	X-Benz.[3]	Tabulated[36]
$\frac{Q_{35Cl}}{Q_{37Cl}}$	1.268745(66)[a] 1.26872(13)[34]	1.271(5)	1.2691(2)	1.26880(4)	1.2688(177)
$\frac{Q_{79Br}}{Q_{81Br}}$	1.19704(10)[b]		1.19697(3)	1.197036(6)	1.1969(162)

[a] Derived from line list in ref. 34. [b] This work.

fragment[41] and is a result of the rough approximation in eqn (14) and errors in the values of electronegativity for the halogens. The χ_{cc} ratios for $^{35}Cl/^{37}Cl$ and $^{79}Br/^{81}Br$ equal the ratios of quadrupole moments. The experimental ratios found for the *o*-toluenes are compared to values determined from spectra of halobenzenes[3] and *p*-halotoluenes[4] in Table 5. All values agree within 2σ and are consistent with the ratios determined from the recommended quadrupole moments in ref. 36.

6 Conclusions

Halogen nuclei are able to serve as direct probe of the arrangement of valence electrons, allowing for conclusions on the reactivity of substituted toluenes to be drawn. Since a chlorine substituent exhibits the most effective interaction due to the largest orbital overlap with the aromatic systems, we focus on the chlorinated aromatic rings in Table 2. While the quite invariant values of group electronegativities reveal no significant change in the σ bonds for all chlorinated species, a comparison of the π-character π_c of the C–Cl bond shows that the strongest interaction with the π-system, typically represented by the mesomeric boundary structures, occurs in *o*-chlorotoluene. Within the concept of substitution effects this indicates a comparably stronger influence of the chlorine substituent on the course of an electrophilic aromatic substitution reaction. In Fig. 5 the product yields of the nitration of all the different monochlorotoluenes are exemplified.

Both substituents, chlorine and methyl, are classified as electron pushing relative to the phenyl ring with their +M and +I effects, respectively. In the case of *m*-chlorotoluene both substituents direct the electrophile towards the same positions. The main product **6** satisfies both, chlorine and methyl directing effect, and the nitro group is introduced in *para*- and *ortho*-positions of the chlorine and methyl substituents, respectively.

For *p*-chlorotoluene the two substituents do not direct towards the same positions anymore. The main product **9**, shows that a large portion of reactants follow the directing effect of the methyl substituent rather than the chlorine (ratio 58 : 42). Surprisingly this changes in *o*-chlorotoluene. Here more product forms that follows the chlorine directing effect (38 : 62).

Interestingly the π-bond character π_c of the C–Cl bond seems to reflect this, by showing a larger π_c for *o*-chlorotoluene than for *p*-chlorotoluene. From this observation it seems plausible that π_c is correlated to a more pronounced mesomeric effect and thus to the observed reaction yields.

We also made an attempt to explain the reaction yields in a more detailed qualitative way, provided in the ESI.† Quantitative predictions of reaction yields might be carried out by use of computational methods, which also allow a more detailed insight into the electronic structure of the molecules involved. An example of a study reproducing accurate quantitative yields is the computational investigation of the nitration of toluene.[44]

The well determined barriers to internal rotation of the methyl group in *o*-halotoluenes follow an increasing trend with the size of the halogen nucleus. This is expected to be caused by the increasing exchange-repulsion. However, a quantitative calculation of exchange-repulsion, electronic, polarisation and dispersion contributions was not carried out and could add some additional insight. Such calculations could be provided by effective fragmented potentials.[45–47] The trend in potential barriers is well reproduced quantum-chemically utilizing the MP2 method. Benchmark setting are the extremely precise ratios of quadrupolar moments for chlorine and bromine isotopes. These can be used to determine the precise quadrupole moment of both isotopes even if the quadrupole moment of only one of them has been determined accurately. Since the series of *o*-halotoluenes as well as *p*-halotoluenes are now complete, future investigations might include the series of *m*-halotoluenes. These will prove to be an experimentally as well as theoretically challenging problem since strong quadrupolar coupling in the presence of very small barrier to internal rotation with significant V_3 and V_6 contributions are apparent. An initial microwave study on *m*-fluorotoluene can already be found in ref. 48 and will be extended to a complete FTMW study on the parent and all singly substituted ^{13}C isotopes.[49] A study of *m*-chlorotoluene was recently published.[42]

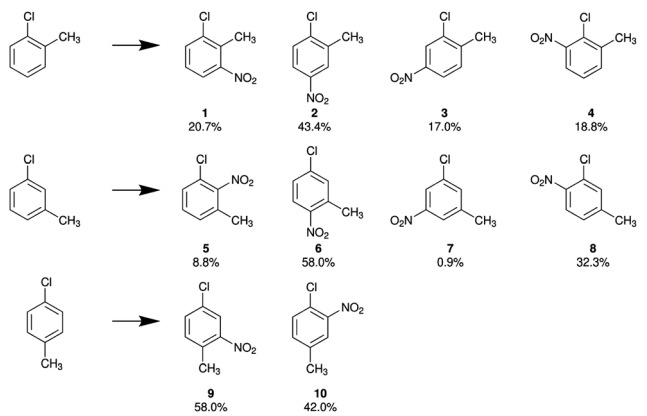

Fig. 5 Observed product yields for the nitration of *o*-, *m*- and *p*-chlorotoluene.[43]

Conflicts of interest

There are no conflicts to declare.

Acknowledgements

J. W. wants to thank the China Scholarships Council (CSC) for financial support. K. G. L. wants to thank the Fonds der

Chemischen Industrie (FCI) for his fellowship. We want to acknowledge the financial support of the Land Niedersachsen, the Deutsche Forschungsgemeinschaft (DFG) and the support of the cluster system team at the Leibniz University IT services (LUIS) Hannover, Germany.

Notes and references

1 M. D. Saltzman, *J. Chem. Educ.*, 1980, **57**, 484.
2 G. A. Olah, Q. Wang, X. Li and I. Bucsi, *Synthesis*, 1992, 1085–1086.
3 O. Dorosh, E. Bialkowska-Jaworska, Z. Kisiel and L. Pszczólkowski, *J. Mol. Spectrosc.*, 2007, **2**, 228–232.
4 V. A. Shubert, D. Schmitz and M. Schnell, *Mol. Phys.*, 2013, **111**, 2189–2197.
5 J. K. G. Watson, *J. Mol. Spectrosc.*, 1977, **65**, 123–133.
6 W. Gordy and R. L. Cook, *Microwave Molecular Spectra*, Wiley, 3rd edn, 1984.
7 J. D. Swalen, *Rev. Mod. Phys.*, 1959, **31**, 841–892.
8 I. Kleiner, *J. Mol. Spectrosc.*, 2010, **260**, 1–18.
9 H. P. Benz, A. Bauder and H. Günthard, *J. Mol. Spectrosc.*, 1966, **21**, 156–164.
10 R. Woods, *J. Mol. Spectrosc.*, 1966, **21**, 4–24.
11 R. Woods, *J. Mol. Spectrosc.*, 1967, **22**, 49–59.
12 H. Hartwig, Dr. rer. nat., dissertation, Christian-Albrechts-Universität Kiel, 1995.
13 H. Hartwig and H. Dreizler, *Z. Naturforsch., A: Phys. Sci.*, 1996, **51a**, 923–932.
14 I. Merke, A. Lüchow and W. Stahl, *J. Mol. Struct.*, 2006, **780–781**, 295–299.
15 M. J. Frisch, G. W. Trucks, H. B. Schlegel, G. E. Scuseria, M. A. Robb, J. R. Cheeseman, G. Scalmani, V. Barone, G. A. Petersson, H. Nakatsuji, X. Li, M. Caricato, A. V. Marenich, J. Bloino, B. G. Janesko, R. Gomperts, B. Mennucci, H. P. Hratchian, J. V. Ortiz, A. F. Izmaylov, J. L. Sonnenberg, D. Williams-Young, F. Ding, F. Lipparini, F. Egidi, J. Goings, B. Peng, A. Petrone, T. Henderson, D. Ranasinghe, V. G. Zakrzewski, J. Gao, N. Rega, G. Zheng, W. Liang, M. Hada, M. Ehara, K. Toyota, R. Fukuda, J. Hasegawa, M. Ishida, T. Nakajima, Y. Honda, O. Kitao, H. Nakai, T. Vreven, K. Throssell, J. A. Montgomery, Jr., J. E. Peralta, F. Ogliaro, M. J. Bearpark, J. J. Heyd, E. N. Brothers, K. N. Kudin, V. N. Staroverov, T. A. Keith, R. Kobayashi, J. Normand, K. Raghavachari, A. P. Rendell, J. C. Burant, S. S. Iyengar, J. Tomasi, M. Cossi, J. M. Millam, M. Klene, C. Adamo, R. Cammi, J. W. Ochterski, R. L. Martin, K. Morokuma, O. Farkas, J. B. Foresman and D. J. Fox, *Gaussian 16 Revision A.03*, Gaussian Inc., Wallingford, CT, 2016.
16 A. D. Becke, *J. Chem. Phys.*, 1993, **98**, 5648–5652.
17 C. Lee, W. Yang and R. G. Parr, *Phys. Rev. B: Condens. Matter Mater. Phys.*, 1988, **37**, 785–789.
18 S. H. Vosko, L. Wilk and M. Nusair, *Can. J. Phys.*, 1980, **58**, 1200–1211.
19 F. J. Devlin, J. W. Finley, P. J. Stephens and M. J. Frisch, *J. Phys. Chem.*, 1995, **99**, 16883–16902.
20 C. Møller and M. S. Plesset, *Phys. Rev.*, 1934, **46**, 618–622.
21 M. N. Glukhovtsev, A. Pross, M. P. McGrath and L. Radom, *J. Chem. Phys.*, 1995, **103**, 1878.
22 K. Schuchardt, B. Didier, T. Elsethagen, L. Sun, V. Gurumoorthi, J. Chase, J. Li and T. Windus, *J. Chem. Inf. Model.*, 2007, **47**, 1045–1052.
23 M. Douglas and N. M. Kroll, *Ann. Phys.*, 1974, **82**, 89–155.
24 B. A. Hess, *Phys. Rev. A: At., Mol., Opt. Phys.*, 1985, **32**, 756–763.
25 B. A. Hess, *Phys. Rev. A: At., Mol., Opt. Phys.*, 1986, **33**, 3742–3748.
26 G. Jansen and B. A. Hess, *Phys. Rev. A: At., Mol., Opt. Phys.*, 1989, **39**, 6016–6017.
27 J.-U. Grabow, W. Stahl and H. Dreizler, *Rev. Sci. Instrum.*, 1996, **67**, 4072–4084.
28 M. K. Jahn, D. A. Dewald, D. Wachsmuth, J.-U. Grabow and S. C. Mehrotra, *J. Mol. Spectrosc.*, 2012, **280**, 54–60.
29 H. M. Pickett, *J. Mol. Spectrosc.*, 1991, **148**, 371–377.
30 S. Jacobsen, U. Andresen and H. Mäder, *Struct. Chem.*, 2003, **14**, 217–225.
31 K. P. R. Nair and K. Epple, *Chem. Phys. Lett.*, 1990, **166**, 146–152.
32 E. C. Richard, R. A. Walker and J. C. Weisshaar, *J. Chem. Phys.*, 1996, **104**, 4451–4469.
33 K. P. R. Nair, *J. Mol. Struct.*, 1999, **477**, 251–254.
34 D. Gerhard, A. Hellweg, I. Merke, W. Stahl, M. Baudelet, D. Petitprez and G. Wlodarczak, *J. Mol. Spectrosc.*, 2003, **220**, 234–241.
35 K. P. R. Nair, J. Demaison, G. Wlodarczak and I. Merke, *J. Mol. Spectrosc.*, 2006, **237**, 137–142.
36 P. Pyykkö, *Mol. Phys.*, 2001, **99**, 1617–1629.
37 M. Meyer, W. Stahl and H. Dreizler, *J. Mol. Spectrosc.*, 1992, **151**, 243–259.
38 C. H. Townes and B. P. Dailey, *J. Chem. Phys.*, 1949, **17**, 782–796.
39 S. E. Novick, *J. Mol. Spectrosc.*, 2011, **267**, 13–18.
40 V. Jaccarino, J. G. King, R. A. Satten and H. H. Stroke, *Phys. Rev.*, 1954, **94**, 1798–1799.
41 W. Gordy, *J. Chem. Phys.*, 1954, **22**, 1470–1471.
42 K. P. R. Nair, S. Herbers, A. Lesarri and J.-U. Grabow, *J. Mol. Spectrosc.*, 2019, **361**, 1–7.
43 H. S. Fry, *J. Am. Chem. Soc.*, 1916, **38**, 1327–1333.
44 Y. Nieves-Quinones and D. A. Singleton, *J. Am. Chem. Soc.*, 2016, **138**, 15167–15176.
45 M. S. Gordon, Q. A. Smith, P. Xu and L. V. Slipchenko, *Annu. Rev. Phys. Chem.*, 2013, **64**, 553–578.
46 M. S. Gordon, D. G. Fedorov, S. R. Pruitt and L. V. Slipchenko, *Chem. Rev.*, 2012, **112**, 632–672.
47 D. Ghosh, D. Kosenkov, V. Vanovschi, C. F. Williams, J. M. Herbert, M. S. Gordon, M. W. Schmidt, L. V. Slipchenko and A. I. Krylov, *J. Phys. Chem. A*, 2010, **114**, 12739–12754.
48 H. D. Rudolph and A. Trinkaus, *Z. Naturforsch.*, 1968, **23a**, 68–76.
49 K. P. R. Nair, *et al.*, unpublished.